
Article:
Sana, H., Ramírez-Agudelo, O.H., Hénault-Brunet, V. et al. (2022) The VLT-FLAMES Tarantula Survey. Astronomy & Astrophysics, 668. L5. ISSN: 0004-6361

https://doi.org/10.1051/0004-6361/202244677

A&A 668, L5 (2022)
https://doi.org/10.1051/0004-6361/202244677

Astronomy & Astrophysics

LETTER TO THE EDITOR

The VLT-FLAMES Tarantula Survey

Observational evidence for two distinct populations of massive runaway stars in 30 Doradus

H. Sana[1], O. H. Ramírez-Agudelo[2], V. Hénault-Brunet[3], L. Mahy[1,20], L. A. Almeida[4,21], A. de Koter[5,1], J. M. Bestenlehner[6], C. J. Evans[7], N. Langer[8], F. R. N. Schneider[9,10], P. A. Crowther[6], S. E. de Mink[11,5], A. Herrero[12], D. J. Lennon[12], M. Gieles[13,14], J. Maíz Apellániz[15], M. Renzo[16], E. Sabbi[17], J. Th. van Loon[18], and J. S. Vink[19]

(Affiliations can be found after the references)

Received 4 August 2022 / Accepted 24 November 2022

ABSTRACT

Context. The origin of massive runaway stars is an important unsolved problem in astrophysics. Two main scenarios have been proposed, namely: dynamical ejection or release from a binary at the first core collapse. However, their relative contribution remains heavily debated.
Aims. Taking advantage of two large spectroscopic campaigns towards massive stars in 30 Doradus, we aim to provide observational constraints on the properties of the O-type runaway population in the most massive active star-forming region in the Local Group.
Methods. We used radial velocity measurements of the O-type star populations in 30 Doradus obtained by the VLT-FLAMES Tarantula Survey and the Tarantula Massive Binary Monitoring to identify single and binary O-type runaways. Here, we discuss the rotational properties of the detected runaways and qualitatively compare the observations with expectations of ejection scenarios.
Results. We identified 23 single and one binary O-type runaway objects, most of them located outside the main star-forming regions in 30 Doradus. We find an overabundance of rapid rotators ($v_e \sin i > 200\,\mathrm{km\,s^{-1}}$) among the runaway population, thus providing an explanation for the observed overabundance of rapidly rotating stars in the 30 Doradus field. Considerations of the projected rotation rates and runaway line-of-sight velocities reveal a conspicuous absence of rapidly rotating ($v_e \sin i > 210\,\mathrm{km\,s^{-1}}$), fast-moving ($v_{los} > 60\,\mathrm{km\,s^{-1}}$) runaway stars in our sample, strongly suggesting the presence of two different populations of runaway stars: a population of rapidly spinning but slowly moving runaway stars and a population of fast-moving but slowly rotating ones. These are detected with a ratio close to 2:1 in our sample.
Conclusions. We argue that slowly moving but rapidly spinning runaway stars result from binary ejections, while rapidly moving but slowly spinning runaways could result from dynamical ejections. Given that detection biases will more strongly impact the slow-moving runaway population, our results suggest that the binary evolution scenario dominates the current massive runaway star population in 30 Doradus.

Key words. stars: early-type – stars: massive – binaries: spectroscopic – stars: rotation – stars: kinematics and dynamics – galaxies: star clusters: individual: 30 Dor

1. Introduction

Massive runaway stars (Blaauw 1961) hurtle through space with speeds of a few tens to a couple of hundreds of $\mathrm{km\,s^{-1}}$. During their lifetimes, they can travel large distances (up to 1000s of pc) from their birthplaces, meaning that they have the potential to inject radiative and mechanical energy as well as processed chemical elements deep into the interstellar – and sometimes intergalactic – medium (Ceverino & Klypin 2009; Andersson et al. 2020).

Two distinct mechanisms have been proposed to explain their origin: dynamical interaction in a dense star cluster (Blaauw 1961; Gies & Bolton 1986) or release from a close binary system when the companion explodes as a supernova (Zwicky 1957; Stone 1991). Both of these are believed to occur in nature (Hoogerwerf et al. 2000), but their relative efficiency as well as the resulting ejection rates and velocity distributions have been a topic of debate over the past 50 years (Blaauw 1961; Hoogerwerf et al. 2001; Jilinski et al. 2010; Dorigo Jones et al. 2020). Understanding these mechanisms and their relative contributions is pivotal for quantifying the feedback of massive stars in the broader context of reionization and the chemical enrichment of galaxies (Conroy & Kratter 2012).

The 30 Doradus region (i.e., 30 Dor) in the Large Magellanic Cloud (LMC) is the nearest strong starburst and it contains one of the richest massive-star populations in the Local Group of galaxies. Therefore, 30 Dor gives us a unique laboratory for obtaining statistically meaningful observational constraints on the properties of massive stars, including those of runaways. In particular, the massive young cluster R136 (at the centre of 30 Dor) is expected to provide a suitably dense environment for dynamical interactions to occur, but is likely too young to have produce any supernova. Moreover, the metallicity of the LMC is ~50% solar (e.g., Banerjee et al. 2012; Lebouteiller et al. 2019), so 30 Dor provides a valuable window into the properties of massive stars in conditions that are comparable to those characterising the peak of star formation in the Universe.

The short lifetimes of O-type stars allow us to obtain a (nearly) real-time snapshot of the production of massive runaways in 30 Dor, while also minimizing possible interlopers that would originate from outside our studied region. Here we employ measurements from multi-epoch spectroscopy of

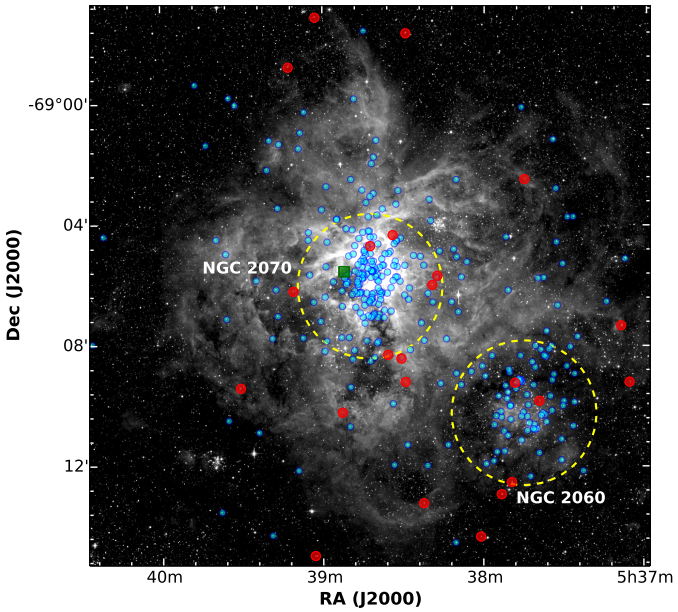

Fig. 1. *V*-band Wide Field Imager (WFI) mosaic of the 30 Doradus region. O-type stars runaways single (red) and binary (green) identified in this work are spread throughout the field of view, while the non-runaway O-type stars (blue circles) cluster within the NGC 2060 and NGC 2070 OB associations (dashed 2.4′-radius circles, equiv. 36 pc in radius).

339 massive O-type stars obtained at the Very Large Telescope (VLT) in the framework of the VLT-FLAMES Tarantula Survey (VFTS; Evans et al. 2011), combined with follow-up spectroscopy obtained over 20 months to monitor 74 of the 118 identified O-type binaries (Almeida et al. 2017). Finally, we contrast the specific line-of-sight velocities ($v_{\rm los}$) of the identified runaways and their projected spins in an attempt to separate out their production channels.

2. Observational data

2.1. The VLT-FLAMES Tarantula Survey

The bulk of the data used in this work were acquired as part of the VFTS (Evans et al. 2011), a 160 h Large Programme at the European Southern Observatory (ESO). Executed from 2009 to 2010, the VFTS obtained multi-epoch optical spectroscopy of 800 OB-type stars in the 30 Dor region. The targets spanned a field 20′ in diameter (≈300 pc) centred on the R136 cluster (see Fig. 1), but avoiding most of the inner 1′-region and, hence, most of R136 itself due to crowding (see, however, Hénault-Brunet et al. 2012, for an attempt to get closer). The data were obtained with the Fibre Large Array Multi-Element Spectrograph (FLAMES, Pasquini et al. 2002), using its Medusa fibres to feed the Giraffe spectrograph with light from up to 132 targets simultaneously. The LR02 and LR03 settings of the low-resolution grating were used to provide continuous coverage of 3960–5050 Å at a spectral resolving power, $\lambda/\Delta\lambda$, of ∼7500. The Hα region was also observed for each target at $\lambda/\Delta\lambda$ = 15 000 with the HR15N setting.

The observations and data reduction were described by Evans et al. (2011). Spectral classification, extinction properties, absolute luminosities, absolute radial velocities (RVs), projected rotational velocities ($v_{\rm e} \sin i$) and atmospheric parameters of the O-type stars in the survey have been presented in various papers in the VFTS series (Sana et al. 2013; Ramírez-Agudelo et al. 2013; Maíz Apellániz et al. 2014; Sabín-Sanjulián et al. 2014; Walborn et al. 2014). Evolutionary parameters (age: τ; current mass: $M_{\rm act}$) were estimated for each object using a Bayesian method that matches selected observational constraints to stellar evolutionary models (Brott et al. 2011), while accounting for the observational uncertainties (Schneider et al. 2018).

O-type spectroscopic binaries and binary candidates were identified from RV variations (Sana et al. 2013). Of the 339 O-type stars observed by the VFTS, 185 showed no statistically-significant RV variations and are presumed to be single stars (although some of them will inevitably be undetected binaries; see additional considerations below on the binary detection completeness). A further 36 stars displayed significant RV variations, but with peak-to-peak amplitudes of less than 20 km s^{-1}. These are either spectroscopic binaries or stars displaying photospheric activity (Almeida et al. 2017; Simón-Díaz et al. 2020). The remaining 118 objects, with peak-to-peak RV variations >20 km s^{-1}, are considered strong spectroscopic binary candidates (Sana et al. 2013).

2.2. The Tarantula massive binary monitoring

Long-term spectroscopic monitoring of 76 of the 118 O-type binary candidates was obtained over October 2012 to March 2014 in the Tarantula Massive Binary Monitoring programme (TMBM, Almeida et al. 2017). This enabled the detailed characterisation of a representative fraction (65%) of the known massive spectroscopic binaries in 30 Dor. The TMBM obtained 32 spectra of each system with the LR02 setting, with the observations sampling timescales of days and weeks up to 20 months.

The data were reduced and RVs were estimated using identical methods to those employed for the VFTS data (Evans et al. 2011; Sana et al. 2013). We measured the orbital periods through a Fourier analysis and adjusted the RV curves to obtain the orbital parameters (Cumming 2004), including a refined orbital period, eccentricity, semi-amplitude of the RV curve, systemic velocity, and ephemeris. Further characterisations of the double- and single-line spectroscopic binaries were reported in Mahy et al. (2020a,b) and Shenar et al. (2022a,b), respectively.

We rejected four systems with tentative orbital periods >510 days (length of the observational campaign) as strong aliasing did not allow us to firmly derive the orbital properties. The resulting estimates of systemic velocities of the remaining 72 binaries allowed us to search for runaway binary systems using the same approach as for single stars.

3. Identifying runaway stars through their peculiar line-of-sight velocity

We identify runaway stars as those with estimated RVs that deviate by more than 3σ from the systemic RV of the O-star population in the survey. Our analysis proceeded as follows. From the 339 O-type objects in the VFTS (Walborn et al. 2014), we selected those without significant RV variations, namely, the 185 presumed single stars. We first measured the systemic and 1σ dispersion of the single stars using the unweighted mean and dispersion of the RV sample and a κ–σ clipping to reject outliers. We also computed generalized RV histograms for the different O-star populations in the observed field, which we fit using Gaussian distributions (Fig. 2). The systemic velocities ($v_{\rm sys}$) and dispersions ($\sigma_{\rm v}$) obtained from these two methods and for the different O-star populations are in excellent

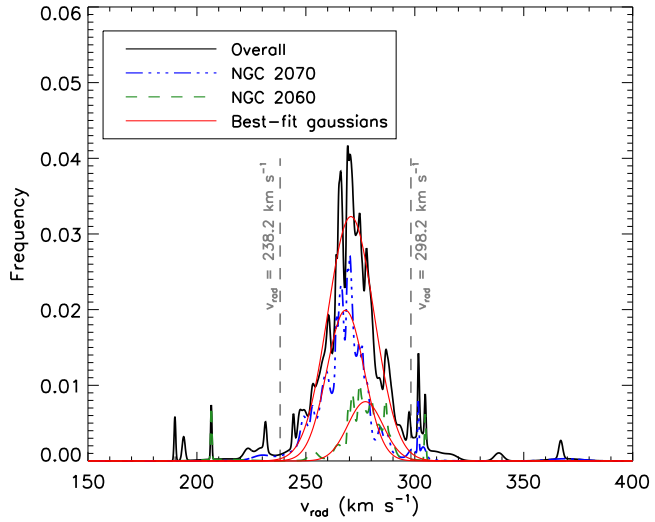

Fig. 2. Generalised line-of-sight velocity histograms of the O-type stars in 30 Dor together with the best-fit Gaussian distribution function (Table 1).

agreement (Table 1). In doing so, we used the same definition of the NGC 2070 and NGC 2060 regions – the two main O-star associations in the 30 dor region – as adopted in the VFTS (Sana et al. 2013). These are displayed in Fig. 1. The population of O star outside the two regions are indicated as 'remaining' in Table 1. In the following, we use the estimate of σ_v obtained from the generalized histograms, as these take into account the individual error bars.

We flagged objects as runaway stars if their line-of-sight velocity (v_{los}) differs by more than 3σ (25.8 km s^{-1}) from the systemic velocity of NGC 2070 (v_{sys}^{2070}), which dominates the O-star population of 30 Dor (Fig. 1). We note that the mean systemic velocities of stars in the NGC 2060 and NGC 2070 differ by $\sim$10 km s^{-1}, but that all the runaways identified below are either outside NGC 2060 or have RVs that differ by more than 3σ from the systemic velocity of NGC 2060. Thus, there is no confusion on their runaway nature, even in the case where NGC 2060 is their parent cluster.

The peculiar line-of-sight velocity (δv_{los}) of the runaway stars (both the single stars and binary systems from the TMBM) is thus given by:

$$\delta v_{los} = |v_{los} - v_{sys}^{2070}| > v_{thres}. \quad (1)$$

In total, 23 (presumed) single stars and one binary meet our RV threshold (v_{thres} = 25.8 km s^{-1}), yielding an observed runaway fraction of 7 ± 1% among the O-type population of 30 Dor, where binomial statistics has been used to compute the observational uncertainties. Adopting the canonical criterion (Hoogerwerf et al. 2000, 2001) of a peculiar velocity larger than 30 km s^{-1} would reduce the number of single runaway stars by two and remove the only qualifying runaway binary system. However, it would not change the conclusions of this Letter. No other runaway stars were identified in the sample with significant RV variations below 20 km s^{-1}.

The spectroscopic binary system that qualifies as a candidate runaway system is VFTS 661 (δv_{los} = 26.4 ± 7.1 km s^{-1}). VFTS 661 is a short period ($P \sim 1.3$ d) detached double-line spectroscopic and eclipsing binary. Unfortunately, the large uncertainty on its systemic velocity, combined with its proximity to the RV threshold, precludes a firm identification.

Most of the identified runaways have peculiar velocities of up to 60 km s^{-1}, but five have even larger velocities of up to 98 km s^{-1} (Table 2). The identified runaways are mostly located outside the two main OB associations in the region, NGC 2060 and NGC 2070 (Fig. 1). The fraction of runaway stars in these regions is 4 ± 2% and 6 ± 2%, respectively, while it reaches 23±5% in the field outside the two associations. This finding is in line with the runaway nature of the objects and strongly suggests that the massive-star field population in 30 Dor is largely composed of stars ejected from the main associations, albeit some of them with a low velocity and/or with unfavourable line-of-sight motions.

The true number of runaway stars in 30 Dor is indeed expected to be much larger as three main observational effects impact our detection: the fact that our selection method is only sensitive to runaway stars that have sufficient line-of-sight velocities ($v_{los} > 25.8$ km s^{-1}), the finite size of our field of investigation (20′ in diameter), and the completeness fraction of the survey ($\sim$0.7). Contamination of our single star sample by undetected binaries would result in false detections, but this latter bias is largely outweighed by the former three effects. Detailed modelling of these biases is beyond the scope of this Letter but a factor of about two to four is to be expected between the detected and true numbers of runaways in the 30 Dor region.

4. Rotational properties of runaway stars

4.1. Projected rotational velocity distribution

We adopted the projected rotational velocities measured in Ramírez-Agudelo et al. (2013) for presumably single O stars. Typical uncertainties are of the order of 20–30 km s^{-1}. Figure 3 shows the cumulative projected spin distributions for stars identified as runaways and those that are not. A Kolmogorov–Smirnov test indicates that the two samples show differences with a significance level better than 5%. The probability of drawing by chance, from the non-runaway sample, a number of fast rotators ($v_e \sin i > v_{cutoff}$) as large as the one observed in the runaway sample drops well below 1% as soon as v_{cutoff} is larger than 200 km s^{-1}. This again suggests that the two distributions differ significantly. The confidence of the results is consistently better than 2.5σ for $v_{cutoff} > 200$ km s^{-1} and even reaches 3σ above 300 km s^{-1}. Thus, there appears to be a cut-off value above which the rotational properties of the runaway and non-runaway populations are incompatible with one another, with the runaway population being preferentially populated by rapidly spinning stars. The overabundance of fast rotators increases exponentially towards larger spinning rates. It is about a factor of two above 200 km s^{-1}, a factor of three above 300, and a factor of six above 400 km s^{-1}.

Interestingly, rapid rotators are more abundant in the single O-star sample outside the NGC 2060 and 2070 OB associations than within these associations. Indeed, 32 ± 6% among the former have $v_e \sin i > 200$ km s^{-1} , with only 20 ± 3% among the latter. It seems therefore plausible that this overabundance of fast rotators outside the main OB associations results from runaway stars spreading across the 30 Dor field of view.

4.2. Rapidly spinning vs. fast-moving runaways

Simultaneous considerations of the projected rotational ($v_e \sin i$) and peculiar line-of-sight (δv_{los}) velocities reveal distinct runaway populations (Fig. 4): a rapidly spinning, slow-moving group and a slowly spinning, fast-moving group. The absence

Table 1. Systemic velocities and 1σ radial-velocity dispersions from the two analysis methods (see text) and runaway (RW) fractions of the single O-star populations in 30 Dor.

Population	Sample size	Sample stat. (km s^{-1})	Gaussian fit (km s^{-1})	RW fraction (%)
Overall	185	271.7 ± 12.6	270.7 ± 10.6	7 ± 1
NGC 2070	90	267.0 ± 9.6	268.2 ± 8.6	6 ± 2
NGC 2060	33	277.5 ± 6.3	277.3 ± 8.0	4 ± 2
Remaining	62	273.2 ± 19.0	272.5 ± 14.8	23 ± 5

Table 2. Properties of the O-type runaway stars detected in 30 Dor.

VFTS ID	Location	v_{los} (km s^{-1})	δv_{los} (km s^{-1})	$v_e \sin i$ (km s^{-1})	Spectral classification	M_{act} ($M_\odot$)	τ (Myr)
012	Out.	316.8 ± 3.0	48.6	306 ± 31	O9 IIIn	$18.8^{+1.1}_{-0.8}$	$5.3^{+0.4}_{-0.5}$
016	Out.	189.9 ± 0.4	78.3	94 ± 30	O2 III-If*	$91.6^{+11.5}_{-10.5}$	$0.7^{+0.1}_{-0.1}$
102	2060	212.0 ± 9.9	56.2	610 ± 61	O9: Vnnne+	$37.2^{+4.6}_{-4.5}$ [b]	<0.9 [b]
138 [a]	Out.	297.7 ± 3.4	29.5	350 ± 35	O9 Vn	$19.4^{+1.2}_{-1.1}$	$1.3^{+1.2}_{-1.3}$
165	2060	206.6 ± 0.3	61.6	75 ± 14	O9.7 Iab	$31.4^{+2.5}_{-3.6}$	$4.6^{+0.4}_{-0.4}$
168	2060	304.8 ± 0.4	36.6	39 ± 20	O8.5 Vz	$23.4^{+1.3}_{-1.0}$	$3.1^{+0.4}_{-0.7}$
190	Out.	223.2 ± 1.7	45.0	444 ± 44	O7 Vnn((f))p	$24.4^{+1.3}_{-2.6}$ [b]	$5.8^{+1.3}_{-1.5}$ [b]
226	Out.	193.9 ± 0.7	74.3	64 ± 10	O9.7 III	$15.6^{+0.6}_{-0.6}$	$2.7^{+1.2}_{-1.45}$
285 [c]	2070	229.6 ± 3.8	38.6	622 ± 62	O7.5 Vnnn	$20.0^{+2.2}_{-1.4}$	$1.9^{+2.5}_{-1.8}$
306	2070	301.6 ± 0.3	33.4	71 ± 10	O8.5 II((f))	$30.4^{+3.3}_{-2.2}$	$4.4^{+0.4}_{-0.4}$
328	Out.	310.3 ± 3.2	42.1	238 ± 10	O9.5 III(n)	$17.2^{+0.8}_{-0.8}$	$1.0^{+1.0}_{-1.0}$
355	Out.	301.9 ± 0.4	33.7	134 ± 26	O4 V((n))((fc))z	$45.8^{+6.7}_{-5.3}$	$1.9^{+0.1}_{-0.1}$
356	Out.	338.5 ± 2.0	70.3	211 ± 42	O6: V(n)z	$28.4^{+3.1}_{-2.9}$	$2.6^{+0.6}_{-0.9}$
370	Out.	231.5 ± 0.6	36.7	68 ± 10	O9.7 III	$16.4^{+0.7}_{-0.8}$	$4.3^{+1.0}_{-1.3}$
406	2070	303.9 ± 1.3	35.7	356 ± 36	O6 nn	$32.0^{+5.3}_{-1.4}$	$3.3^{+1.0}_{-0.4}$ [b]
418 [a]	2070	298.8 ± 0.4	30.6	133 ± 13	O5 V((n))((fc))z	$35.0^{+4.7}_{-3.9}$	$1.3^{+0.6}_{-0.8}$
529 [a]	2070	295.6 ± 10.8	27.4	218 ± 30	O9.5(n)	$17.4^{+1.4}_{-1.2}$	$6.4^{+1.2}_{-1.3}$ [b]
663	Out.	305.4 ± 3.6	37.2	90 ± 10	O8.5 V	$21.0^{+1.9}_{-1.7}$	$2.3^{+1.3}_{-1.6}$
722	Out.	229.4 ± 2.4	38.8	404 ± 40	O7 Vnnz	$23.0^{+1.5}_{-1.8}$	$3.4^{+1.6}_{-1.2}$
724 [a]	Out.	296.8 ± 10.2	28.6	369 ± 30	O7 Vnnz	$24.8^{+5.0}_{-5.1}$	$3.0^{+1.1}_{-2.5}$
755	Out.	301.9 ± 1.6	33.7	286 ± 29	O3 Vn((f*))	$50.8^{+5.4}_{-7.9}$	$1.7^{+0.5}_{-0.7}$
761	Out.	367.0 ± 0.9	98.8	111 ± 10	O6.5 V((n))((f))z	$28.0^{+1.6}_{-1.5}$	$1.2^{+0.6}_{-0.8}$
797 [a]	Out.	297.4 ± 0.6	29.2	138 ± 20	O3.5 V((n))((fc))	$48.6^{+7.2}_{-5.4}$	$1.8^{+0.3}_{-0.3}$
661 [a]	2070	294.6 ± 7.1	26.4	...	O6.5 V(n) + O9.7: V:	26+17	...

Notes. Quoted uncertainties are 1σ errorbars for the velocities (Sana et al. 2013) and 95% confidence interval for the present-day evolutionary masses (M_{act}) and ages (τ) (Schneider et al. 2018), but for VFTS 661, with the mass estimates taken from Mahy et al. (2020a). [a]At 3σ from the mean RV value of the complete and NGC 2070 samples but not for NGC 2060 (also not spatially associated with NGC 2060). [b] Not passing quality checks of Schneider et al. (2018). [c]Also detected in the proper motion study of Platais et al. (2018).

of rapidly spinning fast-moving runaway stars is significant to better than 99% independent of various assumptions that can be made on the parent runaway velocity distributions. This reveals a zone of avoidance in the $v_e \sin i$–δv_{los} parameter space: a runaway desert. The existence of this runaway desert is supported by the *Gaia* DR3 proper motion measurements of our sample stars, as discussed in the Appendix.

5. Discussion and conclusions

Fast rotation is one of the clearest signatures of post-binary interaction systems (Renzo et al. 2019). Under the assumption of continuous star formation, theory predicts (de Mink et al. 2013) that about 19% of the stars might be spun up to $v_e \sin i > 200$ km s^{-1} either through coalescence (5%) or mass-transfer (14%). A small fraction (≈4%) of objects are interacting but not significantly spun up (slow case-A interaction Algol-like systems). Aside from merger products (Schneider et al. 2019, 2020), some post-interaction products may also show modest or moderate rotation, because of inclination effects or a lack of significant accretion in non-conservative mass-transfer cases. Tidal locking in relatively tight binaries may also prevent the secondary from being significantly spun up (Sen et al. 2022). The latter systems are also among those that have the largest orbital velocity, so that a fraction of the high-space velocity runaways may show no significant rotational velocity increase, which is in

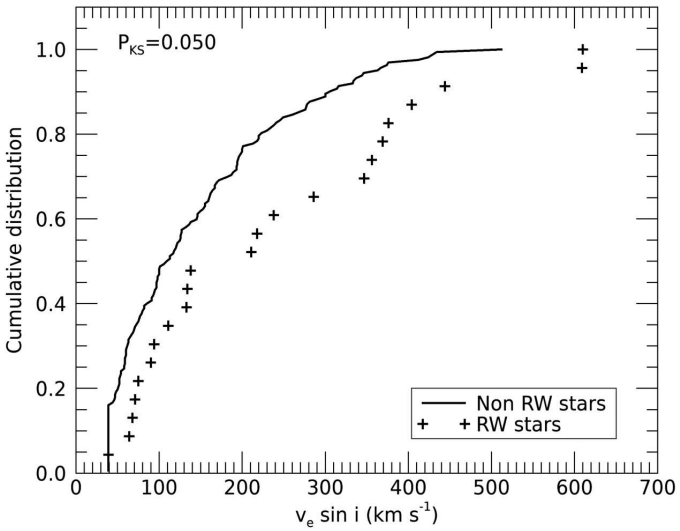

Fig. 3. Cumulative distribution of the projected rotational velocities ($v_e \sin i$) of the runaway stars (+) compared to that of the non-runaway stars (solid curve). Here, P_{KS} indicates the Kolmogorov–Smirnov probability that the two samples are drawn from the same parent distribution.

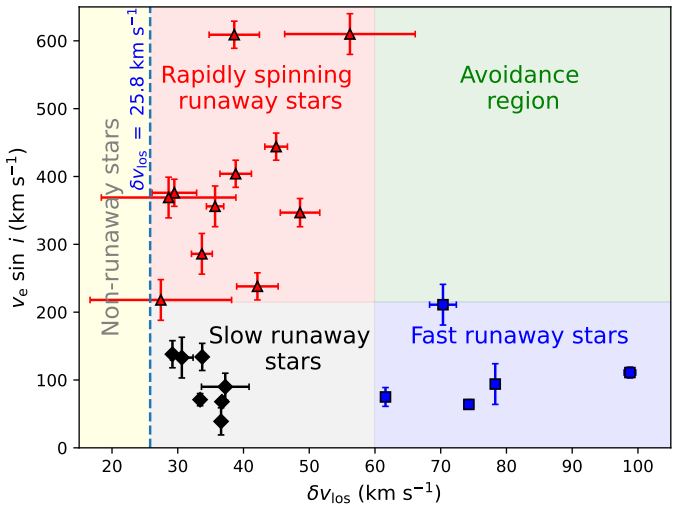

Fig. 4. Diagram of the projected rotational velocities ($v_e \sin i$) vs. peculiar line-of-sight velocities (δv_{los}) for the runaway stars identified in the 30 Doradus region.

qualitative agreement with the distribution of runaway stars in the $v_e \sin i$ versus δv_{los} plane (Fig. 4).

However, the efficiency of producing fast runaways from binary evolution is model-dependent (Eldridge et al. 2011; Renzo et al. 2019; Evans et al. 2020; Sen et al. 2022). Dynamical interactions occur more often in regions of high stellar density (Fujii & Portegies Zwart 2011), pointing to R136 at the core of 30 Dor as the most likely origin. The possible ongoing merger between R136 and Sabbi 1 (Sabbi et al. 2012) suggests R136 was built from sub-clusters with short timescales for dynamical ejection of O-stars (proportional to the relaxation timescale), possibly creating a favourable environment to further contribute to the dynamically ejected runaway population. In either case, and given its young age (Bestenlehner et al. 2020; Brands et al. 2022), it is unlikely that R136 has been ejecting stars for more than 2.5 Myr.

With 55% of the runaway O-star sample displaying $v_e \sin i > 200\,\mathrm{km\,s^{-1}}$ (including the two fastest rotating stars of the entire VFTS sample), the 30 Dor runaway population presents a statistically significant overabundance of rapidly-rotating stars, compared to its non-runaway population (25% with $v_e \sin i > 200\,\mathrm{km\,s^{-1}}$). In addition, the ejection rate of the binary channel increases with age, and the one of the dynamical channel decreases. In regards to the young age of the sample and the fact that detection biases impact comparatively more slow-moving runaways than fast-moving runaways (see Sana et al., in prep.), our results support a predominance of the binary channel in producing the current and future runaway population in 30 Dor. These results contrast with the recent conclusions of Dorigo Jones et al. (2020) on the origin of runaways in the Small Magellanic Cloud (SMC).

Three of our 11 rapidly spinning – likely post-binary interaction – runaway stars have masses in the range of 30–50 solar masses (Table 2). Ignoring dynamical effects, these high masses suggest that at least some dying stars sufficiently massive to form black holes must receive natal kicks that release their companions as runaways. Combined with the recent discovery of X-ray quiet O+BH binaries with significantly different eccentricities (Mahy et al. 2022; Shenar et al. 2022a,b), this would suggest a diversity of collapse scenarios at play. Binary-single and binary-binary exchange interactions in dense clusters can also lead to the ejection of a rapidly rotating stars, reducing the need to invoke BH kicks (Chatterjee & Tan 2012).

Finally, the overall limited contribution of dynamical interaction may be the result of an absence of regions with extremely high stellar density within 30 Dor. This could suggest that R136 only underwent cluster core collapse recently (or not yet), implying a moderate central density at birth. If confirmed, this would challenge the efficiency of massive star formation theories that rely on high stellar densities to significantly contribute to the formation of the most massive stars.

While the *Gaia* DR3 measurements support our results, the current precision does not allow us to trace back most of the runaways to their ejection locus (Platais et al. 2018), other than some rare cases (Evans et al. 2010; Lennon et al. 2018). Future *Gaia* data releases will hopefully provide a sufficient view of stellar motions in the three-dimensional space and provide further observational constraints on their space velocity distribution. Comparisons with the observational properties of the Milky Way runaway population that are being revealed by *Gaia* (Maíz Apellániz et al. 2018) will provide the tools needed to investigate the impact of the environment (metallicity, parent cluster properties, etc.) on the properties of massive-star runaways.

Acknowledgements. This paper is based on data collected at the European Southern Observatory under program ID 182.D-0222, 090.D-0323 and 092.D-0136. The authors are grateful to P. Dufton, M. Kennedy, J. Puls, S. J. Smartt, N. Walborn and to the VFTS consortium for stimulating discussions. The research leading to these results has received funding from the European Research Council (ERC) under the European Union's Horizon 2020 research and innovation programme (grant agreement numbers 772225: MULTIPLES and 945806: TELSTARS). M.A. acknowledges support from the Spanish Government Ministerio de Ciencia through grant and PGC2018-095 049-B-C22. V.H.B. acknowledges the support of the Natural Sciences and Engineering Research Council of Canada (NSERC) through grant RGPIN-2020-05990. M.G. acknowledges support from the Ministry of Science and Innovation (EUR2020-112157, PID2021-125485NB-C22) and from Grant CEX2019-000918-M funded by MCIN/AEI/10.13039/501100011033. L.A.A. thanks the Conselho Nacional de Desenvolvimento Científico e Tecnológico (CNPq) for support through process number 315502/2021-5. FRNS is supported by the Deutsche Forschungsgemeinschaft (DFG, German Research Foundation) under Germany's Excellence Strategy EXC 2181/1-390900948 (the Heidelberg STRUCTURES Excellence

Cluster). This work has made use of data from the European Space Agency (ESA) mission *Gaia* (https://www.cosmos.esa.int/gaia), processed by the *Gaia* Data Processing and Analysis Consortium (DPAC, https://www.cosmos.esa.int/web/gaia/dpac/consortium). Funding for the DPAC has been provided by national institutions, in particular the institutions participating in the Gaia Multilateral Agreement.

References

Almeida, L. A., Sana, H., Taylor, W., et al. 2017, A&A, 598, A84
Andersson, E. P., Agertz, O., & Renaud, F. 2020, MNRAS, 494, 3328
Banerjee, S., Kroupa, P., & Oh, S. 2012, ApJ, 746, 15
Bestenlehner, J. M., Crowther, P. A., Caballero-Nieves, S. M., et al. 2020, MNRAS, 499, 1918
Blaauw, A. 1961, Bull. Astron. Inst. Neth., 15, 265
Brands, S. A., de Koter, A., Bestenlehner, J. M., et al. 2022, A&A, 663, A36
Brott, I., de Mink, S. E., Cantiello, M., et al. 2011, A&A, 530, A115
Cantat-Gaudin, T., & Brandt, T. D. 2021, A&A, 649, A124
Ceverino, D., & Klypin, A. 2009, ApJ, 695, 292
Chatterjee, S., & Tan, J. C. 2012, ApJ, 754, 152
Conroy, C., & Kratter, K. M. 2012, ApJ, 755, 123
Cumming, A. 2004, MNRAS, 354, 1165
de Mink, S. E., Langer, N., Izzard, R. G., Sana, H., & de Koter, A. 2013, ApJ, 764, 166
Dorigo Jones, J., Oey, M. S., Paggeot, K., Castro, N., & Moe, M. 2020, ApJ, 903, 43
Eldridge, J. J., Langer, N., & Tout, C. A. 2011, MNRAS, 414, 3501
Evans, C. J., Taylor, W. D., Hénault-Brunet, V., et al. 2011, A&A, 530, A108
Evans, C. J., Walborn, N. R., Crowther, P. A., et al. 2010, ApJ, 715, L74
Evans, F. A., Renzo, M., & Rossi, E. M. 2020, MNRAS, 497, 5344
Fujii, M. S., & Portegies Zwart, S. 2011, Science, 334, 1380
Gaia Collaboration (Vallenari, A., et al.) 2022, A&A, in press https://doi.org/10.1051/0004-6361/202243940
Gies, D. R., & Bolton, C. T. 1986, ApJS, 61, 419
Hénault-Brunet, V., Evans, C. J., Sana, H., et al. 2012, A&A, 546, A73
Hoogerwerf, R., de Bruijne, J. H. J., & de Zeeuw, P. T. 2000, ApJ, 544, L133
Hoogerwerf, R., de Bruijne, J. H. J., & de Zeeuw, P. T. 2001, A&A, 365, 49
Jilinski, E., Ortega, V. G., Drake, N. A., & de la Reza, R. 2010, ApJ, 721, 469
Lebouteiller, V., Cormier, D., Madden, S. C., et al. 2019, A&A, 632, A106
Lennon, D. J., Evans, C. J., van der Marel, R. P., et al. 2018, A&A, 619, A78
Mahy, L., Almeida, L. A., Sana, H., et al. 2020a, A&A, 634, A119
Mahy, L., Sana, H., Abdul-Masih, M., et al. 2020b, A&A, 634, A118
Mahy, L., Sana, H., Shenar, T., et al. 2022, A&A, 664, A159
Maíz Apellániz, J. 2022, A&A, 657, A130
Maíz Apellániz, J., Evans, C. J., Barbá, R. H., et al. 2014, A&A, 564, A63
Maíz Apellániz, J., Pantaleoni González, M., Barbá, R. H., et al. 2018, A&A, 616, A149
Pasquini, L., Avila, G., Blecha, A., et al. 2002, The Messenger, 110, 1
Platais, I., Lennon, D. J., van der Marel, R. P., et al. 2018, AJ, 156, 98
Ramírez-Agudelo, O. H., Simón-Díaz, S., Sana, H., et al. 2013, A&A, 560, A29
Renzo, M., Zapartas, E., de Mink, S. E., et al. 2019, A&A, 624, A66
Sabbi, E., Lennon, D. J., Gieles, M., et al. 2012, ApJ, 754, L37
Sabín-Sanjulián, C., Simón-Díaz, S., Herrero, A., et al. 2014, A&A, 564, A39
Sana, H., de Koter, A., de Mink, S. E., et al. 2013, A&A, 550, A107
Schneider, F. R. N., Sana, H., Evans, C. J., et al. 2018, Science, 359, 69
Schneider, F. R. N., Ohlmann, S. T., Podsiadlowski, P., et al. 2019, Nature, 574, 211
Schneider, F. R. N., Ohlmann, S. T., Podsiadlowski, P., et al. 2020, MNRAS, 495, 2796
Sen, K., Langer, N., Marchant, P., et al. 2022, A&A, 659, A98
Shenar, T., Sana, H., Mahy, L., et al. 2022a, Nat. Astron.
Shenar, T., Sana, H., Mahy, L., et al. 2022b, A&A, 665, A148
Simón-Díaz, S., Britvaskiy, N., Castro, N., & Holgado, G. 2020, in XIV.0 Scientific Meeting (virtual)., 186
Stone, R. C. 1991, AJ, 102, 333
Walborn, N. R., Sana, H., Simón-Díaz, S., et al. 2014, A&A, 564, A40
Zwicky, F. 1957, Morphological Astronomy (Berlin: Springer)

[1] Institute of Astronomy, KU Leuven, Celestijnlaan 200D, 3001 Leuven, Belgium
e-mail: hugues.sana@kuleuven.be
[2] German Aerospace Center (DLR), Institute for the Protection of Terrestrial Infrastructures, Rathausallee 12, 53757 Sankt Augustin, Germany
[3] Department of Astronomy and Physics, Saint Mary's University, 923 Robie Street, Halifax NS B3H 3C3, Canada
[4] Escola de Ciências e Tecnologia, Universidade Federal do Rio Grande do Norte, Natal 59072-970, Brazil
[5] Anton Pannenkoek Astronomical Institute, University of Amsterdam, 1090 GE Amsterdam, The Netherlands
[6] Department of Physics & Astronomy, Hounsfield Road, University of Sheffield, Sheffield S3 7RH, UK
[7] European Space Agency (ESA), ESA Office, Space Telescope Science Institute, 3700 San Martin Drive, Baltimore, MD 21218, USA
[8] Argelander-Institut für Astronomie, der Universität Bonn, Auf dem Hügel 71, 53121 Bonn, Germany
[9] Heidelberger Institut für Theoretische Studien, Schloss-Wolfsbrunnenweg 35, 69118 Heldelberg, Germany
[10] Astronomisches Rechen-Institut, Zentrum für Astronomie der Universität Heidelberg, Mönchhofstr. 12-14, 69120 Heidelberg, Germany
[11] Max Planck Institut für Astrophysik, Karl-Schwarschild-Strasse 1, 85748 Garching, Germany
[12] Instituto de Astrofísica de Canarias, C/ Vía Láctea s/n, 38200 La Laguna, Tenerife, Spain
[13] ICREA, Pg. Lluís Companys 23, 08010 Barcelona, Spain
[14] Institut de Ciències del Cosmos (ICCUB), Universitat de Barcelona (IEEC-UB), Martí Franquès 1, 08028 Barcelona, Spain
[15] Centro de Astrobiología (-INTA). Campus ESAC, Camino bajo del Castillo s/n., 28 692 Villanueva de la Cañada, Madrid, Spain
[16] Center for Computational Astrophysics, Flatiron Institute, New York, NY 10010, USA Department of Physics, Columbia University, New York, NY 10027, USA
[17] Space Telescope Science Institute, 3700 San Martin Drive, Baltimore, MD 21218, USA
[18] Lennard-Jones Laboratories, Keele University, ST5 5BG Keele, UK
[19] Armagh Observatory, College Hill, Armagh, BT61 9DG Northern Ireland, UK
[20] Royal Observatory of Belgium, Av. Circulaire 3, 1180 Uccle, Belgium
[21] Programa de Pós-graduação em Física, Universidade do Estado do Rio Grande do Norte, Mossoró 59610-210, Brazil

Appendix A: Gaia DR3 proper motions

We retrieved the *Gaia* measurements of the 180 VFTS presumably single O stars from the ARI'Heidelberg Data Release 3 archive (Gaia Collaboration 2022) and applied the corrections recommended by Cantat-Gaudin & Brandt (2021) and Maíz Apellániz (2022). We rejected 32 stars with a Gaia renormalised unit weight error (RUWE) fit quality metric above 1.4. The median measurement uncertainty for the *Gaia* corrected proper motions is 0.07 mas yr^{-1} for our sample, equivalent to $\sim$16 km s^{-1} given the distance to 30 Dor. The proper motion errors are thus significantly larger than the errors on the line-of-sight velocities. Yet, they are small enough to offer a first challenge to the zone of avoidance identified in Fig 4. As for the line of sight velocities, we computed the star proper motion with respect to the central region by subtracting the mean proper motion estimated from the median of 70 stars in a 5″ radius around R136, with good RUWE and parallaxes estimates between 0.017 and 0.025 mas: $pmra_{\rm R136}$ = 1.7003030 mas yr^{-1} and $pmdec_{\rm R136}$ = 0.68414241 mas yr^{-1}. This value is slightly different ($\sim$ 10 km s^{-1}) than that proposed by (Lennon et al. 2018) $pmra_{\rm R136}$ = 1.73863 mas yr^{-1} and $pmdec_{\rm R136}$ = 0.701245 mas yr^{-1}), but it is conveniently between the value of (Lennon et al. 2018) and that obtained from the median of DR3 propper motion of the VFTS single O star sample. Given the likely velocity structure of different regions of the Tarantula nebula (see Table 1), a better precision would require an in-depth investigation that is beyond the present goals.

Figure A.1 (upper row) shows that the runaway desert remains under-populated in the rotational velocity versus right ascension (RA) and declination (Dec.) space velocities. We also computed the space velocities in the tangential plane and the 3D space velocities. Results are displayed in Figure A.1 (bottom row). Unfortunately, the quality of *Gaia* data for the O-type stars is rather inhomogeneous and likely affected by crowding issue for a significant number of objects. Objects with genuinely large plane-of-sky velocities ($>$ 100 km s^{-1}) are challenging to disentangle from objects suffering from crowdedness and other measurement biases (Lennon et al. 2018). The completeness level of 'good' measurements is even harder to asses so that reliable assessment of observational biases based on GAIA data in 30 Dor will have to wait further investigations. Still, the region of avoidance remains underpopulated but for one object (VFTS 615). If the large plane velocity of VFTS 615 ($\sim$ 200 km s^{-1}) is confirmed, this would be the fastest RW object identified in 30 Dor. The reality of this latter finding is far from obvious. Indeed, Platais et al. (2018) combined HST and Gaia data but did not find a significant additional number of rapidly moving massive runaways, confirming once more that our present results are not strongly biased against such objects.

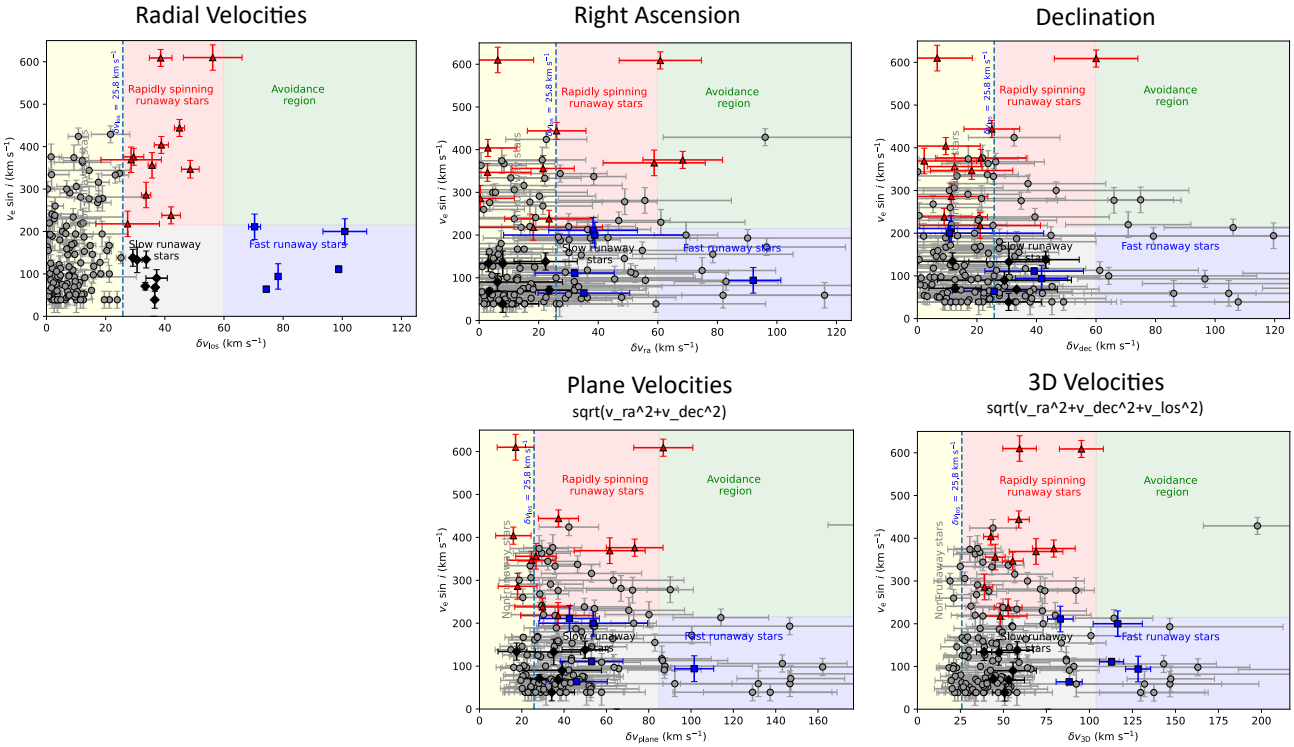

Fig. A.1. Diagram of the projected rotation velocities ($v_{\rm e} \sin i$) versus peculiar 1D space velocities (along the line of sight, RA and DEC on the top row), as well as plane (2D) and 3D peculiar velocities (bottom row) for the full VFTS single O star sample. We exclude 32 objects with GAIA RUWE above 1.4, as this potentially indicate a poor fit or an unresolved system. The boundary of the RW desert obtained via line-of-sight velocities ($v_{\rm e} \sin i > 210$ km s^{-1} and $\delta v_{\rm los} > 60$ km s^{-1}) have been corrected on the bottom row to account for the 2D and 3D nature of the observational constraints using scaling factors of $\sqrt{2}$ and $\sqrt{3}$, respectively. The one object in the avoidance region in the 3D velocities panel displays $\delta v_{dec} \sim 175$ km s^{-1} and $\delta v_{plane} \sim 200$ km s^{-1}, namely, values that are so large that they do not appear on the respective panels.